Fuel 351 (2023) 128945

Contents lists available at ScienceDirect

Fuel

journal homepage: www.elsevier.com/locate/fuel

Full length article

Numerical study on the use of ammonia/hydrogen fuel blends for automotive spark-ignition engines

R. Novella, J. Pastor, J. Gomez-Soriano *, J. Sánchez-Bayona

CMT – Motores Térmicos, Universitat Politècnica de València, Camino de Vera, 46022 Valencia, Spain

ARTICLE INFO

Keywords:
Ammonia
Hydrogen
SI engine
ICE
Virtual engine modelling
Combustion modelling

ABSTRACT

The importance of new alternative fuels has assumed great relevance in the last decades to face the issues of global warming and pollutant emissions from energy production. The scientific community is responsible for developing solutions to achieve the necessary environmental restriction policies. In this context, ammonia appears as a potential fuel candidate and energy vector that may solve the technological difficulties of using hydrogen (H_2) directly in internal combustion engines. Its high hydrogen content per unit mass, higher energy density than liquid hydrogen, well-developed infrastructure and experience in handling and storage make it suitable to be implemented as a long-term solution. In this work, a virtual engine model was developed to perform prospective simulations of different operating conditions using ammonia and H_2-enriched ammonia as fuel in a spark-ignition (SI) engine, integrating a chemical kinetics model and empirical correlations for combustion prediction. In addition, specific conditions were evaluated to consider and to understand the governing parameters of ammonia combustion using computational fluid dynamics (CFD) simulations. Results revealed similar thermal efficiency than methane fuel, with considerable improvements after appropriate H_2-enrichment. Moreover, increasing the intake temperature and the turbulence intensity inside the cylinder evinced significant reductions in combustion duration. Finally, higher compression ratios ensure efficiency gains with no evidence of abnormal combustion (knocking), even at high compression ratios (above 16:1) and low engine speeds (800 rpm). Numerical simulations showed the direct influence of the flame front surface area and the turbulent combustion velocity on efficiency, reflecting the need for optimizing the SI engines design paradigm for ammonia applications.

1. Introduction

It is undeniable that global warming has become one of the biggest problems facing humans beings in modern society. The continuous development of different industrial sectors and the consequent use of fossil fuels contribute directly to the production of greenhouse gases (GHG) such as carbon dioxide (CO_2), hydrocarbons and other pollutants [1]. Transportation is one of the larger contributors to climate change, producing around 32% of global CO_2 emissions in Europe [2]. Moreover, the growth of GHG emissions has continued despite new environmental restriction policies and increasingly efficient vehicles. As a consequence, it is crucial to reduce CO_2 emissions, promoting a transition process towards decarbonization society [3].

Within the decarbonization strategies for energy production various environmentally friendly solutions can be found. For instance, the use of low-carbon fuels (natural gas, alcohols...) or even carbon-free fuels such as ammonia (NH_3) or hydrogen (H_2) [4]. In this context, hydrogen is considered the leading candidate for carbon-free energy vector for both transport and electric power applications [5,6]. However, the use of hydrogen still entails multiple technological difficulties, as well as some inherent drawbacks such as security, infrastructure, storage and performance [7] on internal combustion engines [8]. Recent research advances show that other free-carbon fuels can be considered for different applications for their advantages over hydrogen. Among these, ammonia appears as a potential candidate as an alternative fuel for transportation [9].

Ammonia has a high hydrogen content per unit mass (17.6%) and a volumetric energy density of 15.6 MJ/L in liquid state, higher than liquid hydrogen (around 9.1 MJ/L requiring cryogenic temperatures). Its storage properties are comparable to those of other fuels such as propane [10], being able to condense at atmospheric pressure at −33.4 °C or at ambient temperature (25 °C) from 9.9 atm. Additionally, it has been used for more than hundred years for industrial and agriculture applications, with a well-developed infrastructure and a wealth of experience in storage and handling. All of these aspects make ammonia

* Corresponding author.
E-mail address: jogoso1@mot.upv.es (J. Gomez-Soriano).

https://doi.org/10.1016/j.fuel.2023.128945
Received 13 March 2023; Received in revised form 5 June 2023; Accepted 6 June 2023
Available online 20 June 2023

Nomenclature

AMR	Adaptive Mesh Refinement
BDC	Bottom Dead Center
CAD	Crank Angle Degree
CFD	Computational Fluid Dynamics
CH_4	Methane
CO_2	Carbon Dioxide
CR	Compression Ratio
DNS	Direct Numerical Simulation
EGR	Exhaust Gas Recirculation
GHG	Greenhouse Gases
HRR	Heat Release Rate
ICE	Internal Combustion Engine
IMEP	Indicated Mean Effective Pressure
ISFC	Bottom Dead Center
IVC	Intake Valve Closing
LES	Large Eddy Simulation
LHV	Low Heating Value
NH_3	Ammonia
PFI	Port Fuel Injection
PISO	Pressure-Implicit with Splitting of Operators
RANS	Reynolds-averaged Navier–Stokes
RNG	Re-Normalisation Group
SI	Spark-ignition
ST	Spark Timing
URANS	Unsteady Reynolds-averaged Navier–Stokes

an attractive fuel as a mid-term solution that also synergies with the development of H_2-based economy.

The possibilities of ammonia as an alternative fuel generated interest among both industry [11] and scientific community [12]. Some investigations focused on understanding the fundamental aspects of NH_3 combustion [13] whereas other ones evaluate the use of ammonia as an innovative fuel for shipping, heavy-duty truck transport [14] or even power generation [15].

The use of ammonia in road transport – powered by spark-ignition (SI) engines – still presents some particular challenges to overcome [16]. Toxicity, which is probably its main drawback, can be compensated by the extensive knowledge about handling and storage [17] that exists due to the long experience in agriculture, refrigeration and chemical industry. As a more specific risk, a possible leakage in case of an accident could be harmful for different living species. However, new research works [18] showed that this problem can be avoided by innovative storage methods based on solid-state metal ammine complexes. Finally, its low flame propagation velocity under engine conditions hinder the combustion stability.

In this scenario, hydrogen can be used as an additive for combustion enhancement. Its wide flammability limits, low minimum ignition energy and high flame speed promote the flame stability. In addition, it can be produced on-board by the dissociation of ammonia [19,20]. There are other strategies that involve combining the pre-chamber ignition system [21] with pure ammonia [22] and/or hydrogen mixtures [23] to enhance the ammonia burning rate.

A multitude of research investigations have focused on the combustion of pure ammonia as well as hydrogen-enriched combustion, covering a broad spectrum of fundamental aspects as well as practical applications within the realm of transportation. Tamadonfar et al. [24] visualized the flame dynamics and structure of ammonia/hydrogen/air mixtures. Yang et al. [25] studied the combustion features of ammonia and ammonia-hydrogen fuel blends by means of direct numerical simulation (DNS) and detailed chemistry. Abdelwahid et al. [26] performed extensive computational simulations utilizing large eddy simulation (LES) techniques to explore the intricate interplay between turbulence and chemistry in ammonia-hydrogen jet flames. Wang et al. [27] numerically assessed the combustion performance by a combination of thermodynamic and chemical kinetic calculations. Results of these investigations showed that combustion features are comparable to hydrocarbon fuels under engine-relevant conditions.

Other authors focused on evaluating the impact of NH_3-H_2 blends in SI engines. Xin et al. [28,29] optimized the engine scavenge for an hydrogen-enriched ammonia engine operating at steady-state conditions. Mounaïm-Rousselle et al. [30] demonstrated that pure NH_3 combustion can be used over a large range of engine operating conditions. Lhuillier et al. [31] evaluated their application in a SI engine operating at two different load points under a wide range of hydrogen percentages and equivalence ratios. Their results also showed similar performance to those of conventional fuels when using a controlled testing environment through single-cylinder engines.

The aforementioned studies have significantly enhanced our understanding of various aspects of ammonia combustion and engine operation that were previously unexplored. Nonetheless, certain aspects related to engine architecture, such as compression ratio, boosting system requirements, and combustion system design, as well as additional operating parameters, including combustion control and phasing, have yet to be investigated.

The main objective of this investigation is to evaluate the effect of NH_3 and NH_3-H_2 blends as fuel in a SI engine over a wide range of operating conditions and engine configurations. The study specifically focuses on investigating the necessary modifications that current ICE platforms require to adapt and optimize them for the utilization of ammonia as a fuel. It aims to identify the most promising conventional strategies and provide reasonable ranges of variation. By addressing previously unexplored aspects, the study aims to play a pivotal role in facilitating the adoption of ammonia as a viable transportation fuel. For this purpose, a virtual engine model was used to avoid expensive experiments, safety issues, specific material and qualified personnel. The combustion modelling approach is based on a combination of chemical kinetic calculations and the semi-empirical correlations obtained by Lhuillier et al. [31]. Additionally, 3D CFD simulations were also performed to further understand some particular aspects of the turbulence-combustion coupling.

2. Experimental apparatus and modelling tools

2.1. Engine and test cell characteristics

The experimental facilities used for validation were widely described in previous investigations [32]. Therefore only a brief description of their main features is presented in this work. A single-cylinder SI engine specifically designed for research purposes was used as a reference for the numerical model. The engine was assembled in a fully instrumented test cell and equipped with a port fuel injection (PFI) system. This engine architecture represents a good example for future research applied to ammonia combustion due to its flexibility to switch between two different direct injection locations (cylinder axis center or side injection) or to combine the experiments with optical techniques. Table 1 shows the main specifications of the engine.

A 0D combustion diagnosis tool [33] was used in combination with the experiments to characterize the combustion process and engine outputs. This software estimates the most relevant global parameters related to the combustion process, such as the indicated gross mean effective pressure (IMEP), start of combustion (SoC), combustion phasing (CA50), combustion duration (CA1090), maximum cylinder pressure, combustion stability, heat release rate (HRR) or cylinder mean gas temperature from the measured in-cylinder pressure considering some simplifications to the energy equation. The code assumes uniform pressure and temperature throughout the whole combustion chamber volume to accurately estimate the energy released by combustion.

Table 1
Main engine specifications.

Number of cylinders	1
Ignition system	Spark plug
Number of strokes	4
Cylinder displacement	454.2 cm^3
Compression ratio	10.7
Cylinder diameter	82.0 mm
Stroke	86.0 mm
Connecting rod length	144.0 mm
Valves per cylinder	2 intake, 2 exhaust

2.2. Virtual engine model: description and assessment

The complete test cell layout was implemented the GT-SUITE v2020 code, achieving a good trade-off between accuracy and computing time [34]. This model was originally developed for previous investigations [35] and re-adapted for ammonia-hydrogen fuel blends. Experimental results from 9 operating points (detailed in Table 2) fuelled with methane, were used to validate the virtual engine model. As it can be seen, these points gather the most relevant operating conditions of a current production SI engine. In all these cases, the operating parameters such as ignition timing or injection were optimized to minimize the fuel consumption. The load targets were established by operating the engine with a stoichiometric methane mixture. Once the desired load level was achieved, the fuel energy was calculated based on the injected mass of methane and its Low Heating Value (LHV). Subsequently, the injected NH_3 (or H_2-enriched NH_3) fuel mass was adjusted to maintain the same energy available for combustion at that particular load level and dilution conditions.

As a result, the amount of NH_3 injected fuel mass is increased when switching from methane fuel operation. For an equivalent methane condition, the amount of NH_3 is 63% higher. Similarly, the amount of total injected fuel blend (H_2 + NH_3) is reduced respect to the NH_3 case as the hydrogen percentage is increased in the fuel blend due to its higher LHV. Furthermore, it should be noted that under these conditions, the IMEP level may vary if the thermal efficiency changes due to modifications in other parameters, such as the dilution ratio, compression ratio or combustion phasing.

To minimize the inherent uncertainties of the virtual model, the authors used experimental data from previous investigations [36] to establish the different boundary conditions. Specifically, the ambient pressure and temperature, the coolant temperatures, and the exhaust back-pressure were maintained at the reference values measured in the referenced investigation. Only the intake pressure was modified to achieve the required air mass flow, while the amount of fuel blend was kept constant to maintain equivalent energy for combustion. Therefore, the air mass flow was adjusted by modifying the boosting pressure to achieve the required air-to-fuel ratio.

The combustion process was modelled by imposing directly the combustion profile (HRR) obtained from the experiments and after applying the combustion diagnosis tool at each specific operating condition. This procedure helps to calibrate the convective heat transfer without the uncertainties related to the combustion process. Therefore, each operating condition uses its own optimized combustion settings. The reference combustion settings were subsequently re-optimized by transitioning to ammonia or H_2-enriched ammonia, adjusting the start of combustion and scaling the duration of combustion, as explained in detail below.

Validation results are summarized in Fig. 1. Here, the indicated efficiency levels are contrasted against the experiments. As it can be seen, there is a difference between the predictions and the experiments. This difference remains constant in all operating conditions with an error below 5%, therefore showing a consistent response of the model in all operation conditions. In addition to this, a comparison of the

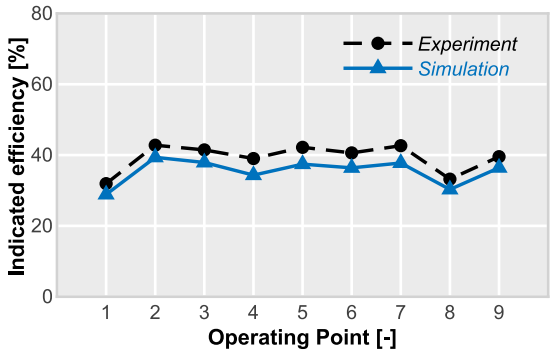

Fig. 1. Validation of the virtual model. The indicated efficiency levels obtained from simulations are contrasted with the experiments performed with methane fuel.

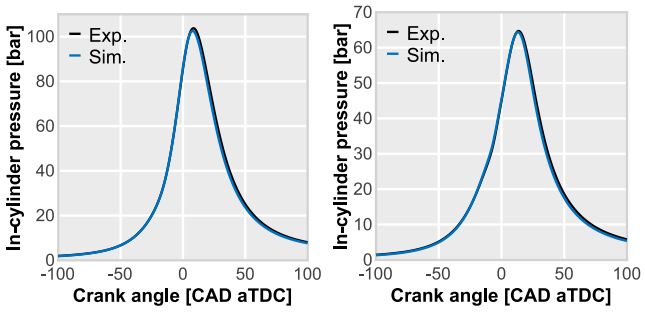

Fig. 2. Validation of the virtual model. Comparison of experimental and simulated in-cylinder pressure profiles for two operating points.

in-cylinder pressure signals obtained from the experiments and simulations was performed highlight the reliability of the virtual model. Fig. 2 shows this comparison for points 2 and 9, being the most extreme conditions of the engine map. As it can be seen, the model accurately reproduces the pressure trend in both operating conditions, also showing similar performance in the other 10 operating points considered (refer to Appendix A).

2.3. CFD model setup

In addition to the experiments, a 3D CFD model was also developed for providing additional data for the virtual model and to help in the understanding of some specific trends and processes observed in NH_3 combustion. The model was implemented in the commercial code CONVERGE version 2.4.33 [37].

The meshing strategy is based on a hexahedral discretization in orthogonal basis with a base cell size of 4 mm. The original mesh size was reduced up to 2 mm in the intake and exhaust ports and up to 1 mm in the combustion chamber. An additional discretization was applied in the vicinity of the cylinder walls reducing the cell size up to 0.5 mm even in the moving parts such as the piston and valves. A mesh resolution of 0.0625 mm was used at the spark electrode, where flame kernel is developed. Additionally, an adaptive mesh refinement (AMR) algorithm was employed to consider the areas where significant temperature or velocity gradients appear. This algorithm increases the mesh resolution up to 0.125 mm based on a sub-grid criteria of 2.5 K for the temperature and 1 m/s for the velocity fields.

This mesh configuration and model setup is well-optimized for SI engine simulations as numerous investigations demonstrated [38,39]. A brief summary of the model configuration, including mesh details, numerical schemes, and the most significant physical models, is shown in the Table 3.

Table 2
Operating parameters of the experimental test conditions used for the validation of the virtual engine model using conventional SI combustion under stoichiometric methane-air conditions.

Operating point	Point 1	Point 2	Point 3	Point 4	Point 5	Point 6	Point 7	Point 8	Point 9
Engine speed [rpm]	4000	4000	3500	2500	2500	2000	2000	1250	1250
IMEP [bar]	2.3	11	6.7	4.4	9.3	6.6	10.6	2.4	8.2
Injected fuel (CH_4) [mg/cc]	6.96	25.50	16.07	11.70	22.45	16.50	25.38	7.28	20.44
SoC [CAD]	−26	−30.8	−23.2	−22.2	−22.4	−19	−20.6	−20.2	−14.2
CA50 [CAD]	4.9	3.4	8.0	8.8	7.1	7.4	6.9	7.1	10.2
Coolant temperature [°C]	87.0	89.0	88.1	87.8	88.6	88.0	88.6	84.0	88.0
Oil temperature [°C]	81.9	81.8	81.9	81.9	82	81.8	81.7	81.8	81.9
Intake pressure [bar]	0.496	1.841	1.084	0.789	1.409	1.043	1.544	0.512	1.172
Intake temperature [°C]	29.02	29.86	28.82	30.48	28.43	31.62	28.82	29.29	28.2

Table 3
CFD model description: mesh characteristics, numerical schemes and physical submodels.

Mesh details	
Base size	4 mm
Cell size intake/exhaust ports	2 mm
Combustion chamber	1 mm
Walls refinement	0.5 mm
Minimum cell size by AMR	0.125 mm
Spark plug refinement	0.0625 mm
Numerical schemes	
Spatial discretization	2nd order central difference scheme
Temporal discretization	1st order central difference scheme
Pressure-velocity coupling	PISO algorithm [40]
Physical models	
Turbulence	URANS RNG k−ϵ [41]
Combustion	G-equation model [37,42]

The Unsteady Reynolds-Averaged Navier Stokes (URANS) based re-normalized group (RNG) k-ϵ model [41] was employed to model turbulence, which was coupled with the wall heat transfer model developed by O'Rourke and Amsden [43]. The compressible flow properties were calculated using the Redlich-Kwong equation of state [44]. A modified Pressure Implicit with Splitting of Operators (PISO) method [40] was used for pressure-velocity coupling.

For combustion modelling, the G-equation model [42] has been adopted for combustion modelling. This approach allows describing the flame propagation based on the flamelet theory of turbulent premixed combustion. The parameter G represents the distance to the flame front, in the form of a non-reacting passive scalar, allowing a tracking by the following transport equation [45]:

$$\frac{\partial \rho \tilde{G}}{\partial t} + \frac{\partial \rho \tilde{u_i} \tilde{G}}{\partial x_i} = -D_T \kappa \left| \frac{\partial \tilde{G}}{\partial x_i} \right| + \rho_u s_T \left| \frac{\partial \tilde{G}}{\partial x_i} \right| \quad (1)$$

where u_i is instantaneous velocity, ρ and ρ_u are the density of the cell and the unburnt density respectively, s_T is the turbulent flame speed, κ is the mean flame front curvature, ˜ stands for the Favre filtering, and D_T represents the turbulent diffusion.

In addition, the turbulent flame speed s_T is calculated in the RANS framework as follows [42]:

$$s_T = s_L + u' \left\{ -\frac{a_1}{2b_1} Da + \left[\left(\frac{a_1}{2b_1} Da \right)^2 + a_1 Da \right]^{1/2} \right\} \quad (2)$$

where u' is the turbulent velocity fluctuation, s_L is the laminar flame speed, Da is the Damköhler number, and a_1 and b_1 are modelling constants. A more detailed description can be found in the following Refs. [37,42].

The laminar flame speeds of the air/fuel mixture, necessary for the combustion model, were obtained using a 1D flamelet code and subsequently stored in tables. This code calculates the flame speed of the combustion reaction by analyzing a freely propagating flame in a channel with a fixed cross-sectional area, considering specific conditions such as temperature, pressure, equivalence ratio, and composition. To maintain consistency with the experimental data, the chemical kinetic mechanism developed by Otomo et al. [46] was employed.

Since detailed chemistry is not resolved, the G-Equation model necessitates an additional model to consider end-gas auto-ignition combustion. In this regard, the SAGE detailed chemistry solver [37] is employed in the unburned region to simulate the auto-ignition delay for the air-fuel blend and subsequent combustion. The mechanism proposed by Otomo et al. [46] was employed to ensure consistency with the calculations of laminar flame speed.

3. Methodology

Once the different models used for the simulations were presented and after validating the virtual engine model by replicating the most relevant operating conditions, the methodology designed for prospective activities of NH_3 and NH_3 + H_2 combustion is presented.

As described above, achieving stable and efficient combustion of ammonia entails several challenges due to its high autoignition temperature and narrow flammability range [47]. Therefore, different strategies were planed to minimize the error of predictions

First, simulations were performed with pure ammonia as fuel for a representative range of engine speeds and loads using the virtual engine model. The objective is to identify the possible changes in the engine operation when switching between conventional and ammonia fuels. In this way, the changes in thermal efficiency, fuel consumption as well as intake/exhaust pressure and temperature will be analysed in detail.

Once the key aspects of ammonia operation were identified, the second step will focus on several strategies to improve and to optimize the engine definition:

- Due to the high knock resistance of ammonia, the impact of increasing the compression ratio (CR) was analysed. To this end, the virtual engine model was combined with CFD simulations, offering a higher level of detail about the physical processes governing ammonia combustion.
- The role of turbulence in achieving faster and more stable combustion was assessed. Again, detailed CFD simulations were performed to study the effect of the tumble intensity on the combustion performance.
- The influence of the intake temperature was studied as it directly affects the laminar flame speed and subsequently, the burning rate [48].
- The effect of H_2-enrichment was evaluated by considering different percentages in the fuel blend.

3.1. Combustion modelling

After validating the virtual engine model using the HRR profiles obtained directly from the experiments presented in Table 2, further actions are needed for mimicking ammonia combustion features in a predictive way. To this end, a new methodology that combines an estimation of the laminar flame speed (s_L) and the semi-empirical correlations obtained by Lhuillier et al. [31] was developed.

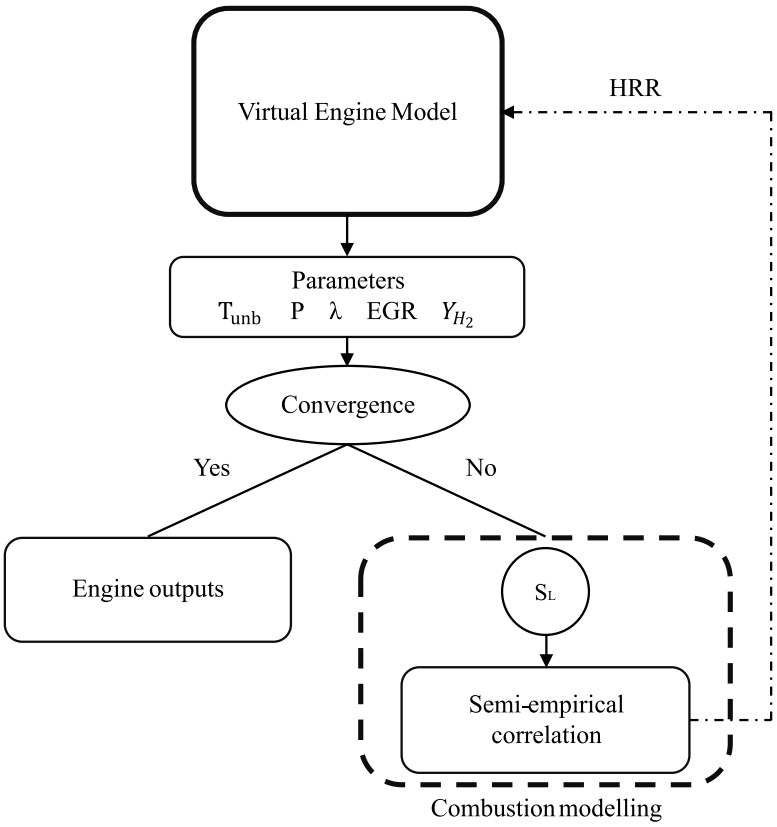

Fig. 3. Coupling between the virtual engine model and the combustion modelling approach.

The method is based on an iterative process that combines the virtual engine model with calculations of laminar flame speed and semi-empirical correlations. The procedure is illustrated in Fig. 3. First, the virtual engine model is run using the reference combustion profile obtained from methane tests. Then, the thermodynamic variables (pressure and temperature) and mixture-related variables (air-to-fuel ratio, EGR, and fuel properties) are obtained at the start of combustion and used as input for the laminar flame speed calculations. The laminar flame speed is computed using the chemical tools available in CONVERGE [37], considering a freely propagating flame in a simulated channel with a fixed cross-sectional area under laminar conditions. The chemical kinetic mechanism developed by Otomo et al. [46] was selected due to its good performance for different air-to-fuel ratio (λ) conditions when considering ammonia and hydrogen fuel blends, and to ensure consistency with the CFD simulations. This mechanism consists of 204 chemical reactions with 32 species and can be used in a wide range of conditions.

The calculated laminar flame speed is used as input for the correlation proposed by Lhuillier et al. [31]. This equation estimates the combustion duration between 10% and 90% of the fuel burnt (CA1090), directly from the laminar flame speed as:

$$CA1090 = \alpha_1 + 20.0037 \cdot e^{-11.7506 \cdot (s_L - \alpha_2)} + 27.9146 \cdot e^{-0.5374 \cdot (s_L - \alpha_3)} \quad (3)$$

The calibration parameters, denoted as α_1, α_2, and α_3, are constants which correlate the thermo-chemical properties within the cylinder with the turbulent properties specific to the engine employed by Lhuillier. These calibration parameters were fine-tuned to match the tumble intensity between Lhuillier's engine and the one utilized in this study. To achieve this, multiple CFD simulations were conducted under motoring conditions at various engine speeds. The resulting calibration parameters are summarized in Table 4.

After calculating the combustion duration using the correlation, a new iteration was conducted with the virtual engine model. In this iteration, the HRR profile utilized in the previous iteration was adjusted to accommodate the new CA1090, taking into account the updated thermo-chemical properties resulting from ammonia engine operation. This iterative procedure maintains the total energy released by the fuel at each operating point. Consequently, the HRR profile was scaled to deal the new combustion duration while preserving the total energy released, achieved by adjusting the maximum HRR peak profile. Additionally, the combustion phasing was maintained by fine-tuning the start of combustion through spark timing (ST). Fig. 4 illustrates the HRR results of the iterative procedure for operating point 12, starting from the reference profile in the first iteration and progressing to the final profile obtained after 5 iterations. The convergence is rapidly achieved, typically requiring only 2–3 iterations to ensure alignment of the HRR profiles. The results of the remaining operating points are included in Appendix B for reference.

Table 4
The calibration parameters for the semi-empirical correlations used in combustion modelling.

α_1	α_2	α_3
5.9981	0.1002	0.0999

3.2. Operating conditions

Twelve operating points, including those used for the validation of the virtual engine model, were considered for the analysis. In this way, a wide range of operating points equivalent to realistic engine conditions was studied. Table 5 shows the main operating parameters used in each operation condition and fuel specification.

In addition to these nominal conditions, the operation condition number 12 was used to evaluate the impact of other parameters such as intake temperature, compression ratio and tumble intensity. The range of variation for each considered parameter is shown in Table 6.

Table 5
Operating conditions for simulations at stoichiometric conditions. CH_4, NH_3 and NH_3 enriched with H_2 (2.5%, 5% and 10% by mass).

Operating point	1	2	3	4	5	6	7	8	9	10	11	12
Engine speed [rpm]	4000	4000	3500	3250	2500	2500	2500	2000	2000	2000	1250	1250
IMEP [bar]	2.3	11	6.7	10	2.3	4.4	9.3	6.6	10.6	9.1	2.4	8.2
CA50 [CAD]	4.9	3.4	8.0	8.0	8.8	8.8	7.1	7.4	6.9	6.9	7.1	10.2
CH_4 [mg/cc]	6.96	25.50	16.07	24.00	7.00	11.70	22.45	16.50	25.38	22.00	7.28	20.45
NH_3 [mg/cc]	18.67	68.38	43.10	64.36	18.77	31.37	60.20	44.24	68.07	58.99	19.52	54.81
NH_3+$H_2^{2.5\%}$ [mg/cc]	16.44	60.2	37.94	56.66	16.53	27.61	52.99	38.95	59.93	51.94	17.18	48.25
NH_3+$H_2^{5\%}$ [mg/cc]	14.66	53.69	33.84	50.53	13.84	24.63	47.27	34.74	53.45	46.32	15.33	43.04
NH_3+$H_2^{10\%}$ [mg/cc]	12.1	44.3	27.92	41.69	12.16	20.32	39.0	28.66	44.1	38.22	12.65	35.51

Table 6
Range of variation for the different parameters studied.

		Case 1	Case 2	Case 3
Engine speed [rpm]	IMEP [bar]	In-cylinder temperature at IVC [°C]	Compression ratio [–]	Tumble ratio [–]
1250	10	[90–130]	[10.7–20]	[0.5–1.9]

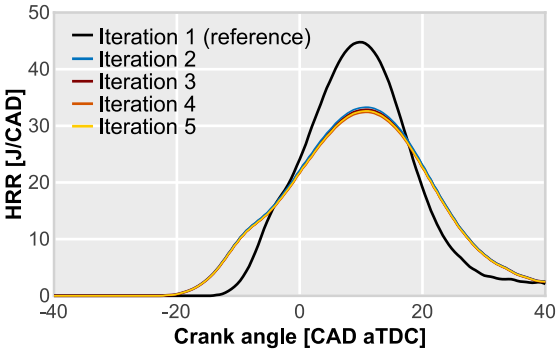

Fig. 4. Results for the convergence of HRR profile for operating point 12.

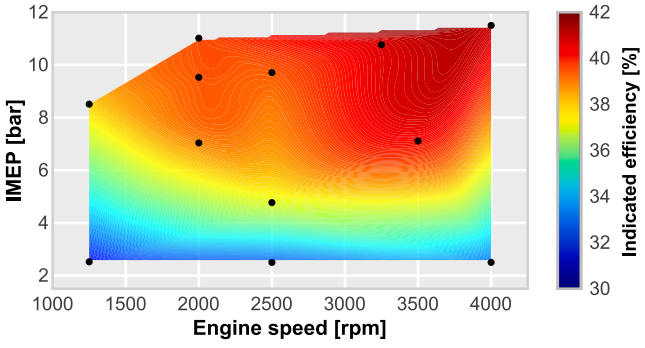

(a) NH_3

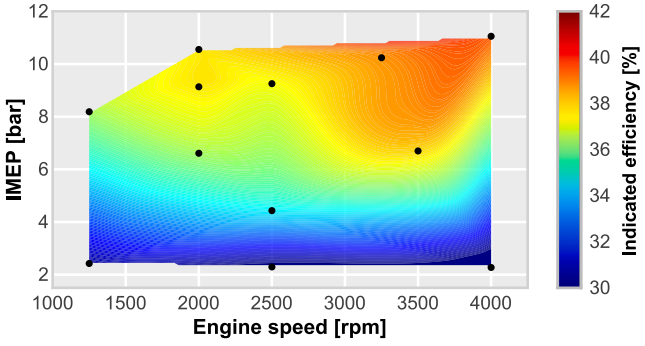

(b) CH_4

Fig. 5. The indicated efficiency levels obtained through the engine map using ammonia and methane fuels are shown in (a) and (b), respectively.

4. Results and discussion

The following section presents the results obtained from the application of the proposed numerical methodology. The analysis is split in two subsections which focus on ammonia combustion and potential strategies for efficiency improvement, and ammonia-hydrogen blends.

4.1. Ammonia combustion

Focusing on thermal efficiency, results of indicated efficiency levels obtained from the simulations are shown in Fig. 5. This graph compares the results of NH_3 operation with equivalent conditions fuelled by methane, both cases operating at stoichiometric conditions (see Table 5 for further details). Inspection of these maps reveals an analogous trend in both fuels. However, NH_3 cases show higher efficiency levels if compared with their equivalent CH_4 conditions (almost 2% of gain).

Such gains are justified by a lower wall heat transfer during expansion when using ammonia as fuel. This effect can be observed in Fig. 6, where the percentage of energy available for propulsion (indicated) and the heat transfer to the chamber walls are computed with respect of the total energy available in the fuel. In general terms, the heat transfer is reduced leading to an increase of the indicated efficiency at all operating conditions.

Concerning the new operating setting under which the engine would operate with ammonia fuel, Fig. 7 shows the required intake pressure and the exhaust temperature variations with respect to the equivalent operating point using methane fuel. Focusing on Fig. 7(a), it can be observed that the intake pressure has to increase to deal with the operating constraints at all operating points. As expected, there is a relationship with the engine load resulting in maximum boost increase of 0.15 bar at full load conditions. According to Fig. 7(b), the exhaust temperature was reduced with respect to the methane cases, with a maximum decrease of 77.2 K at full load and maximum speed. These results evince the need to optimize the boosting system to deal with the expected specifications and efficiency values.

Regarding the combustion process, it is possible to analyse the effect of using ammonia as fuel. To this end, Fig. 8 shows the HRR obtained for operating point 12 (see Table 5) after applying the proposed numerical methodology. In addition, the reference HRR using methane is included for comparison. As it can be seen, the combustion process of NH_3 is slower than CH_4, showing the same tendency in all operating points (data of the other operating points is not included for simplicity).

In addition, it can be observed that the start of combustion and thus, the spark timing (ST), is advanced to keep the same combustion phasing

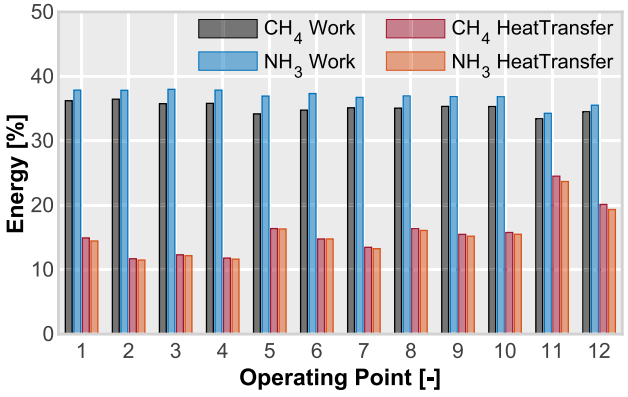

Fig. 6. Energy balance inside the combustion chamber for the 12 operating conditions considering both fuels.

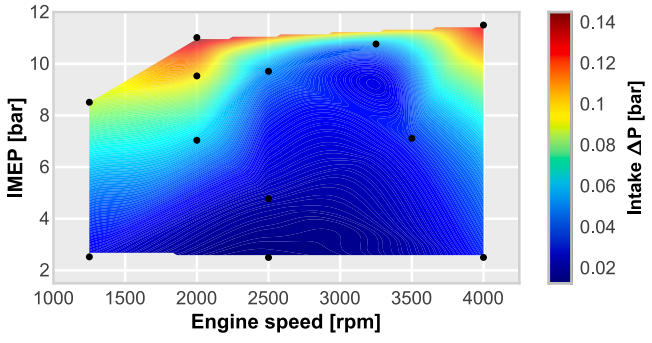

(a) Intake Δp NH_3

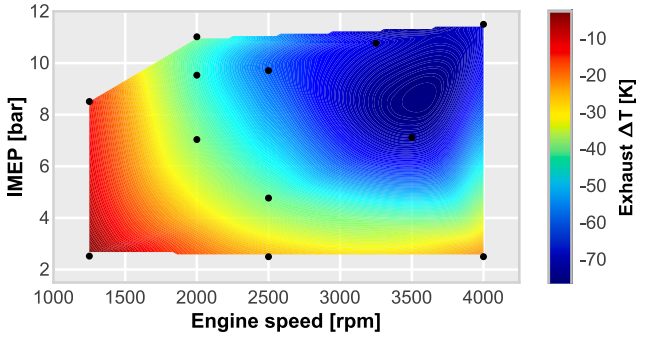

(b) Exhaust ΔT NH_3

Fig. 7. Variation of intake pressure and exhaust gas temperature between the methane and ammonia virtual engine simulations for the operating points defined in Table 5.

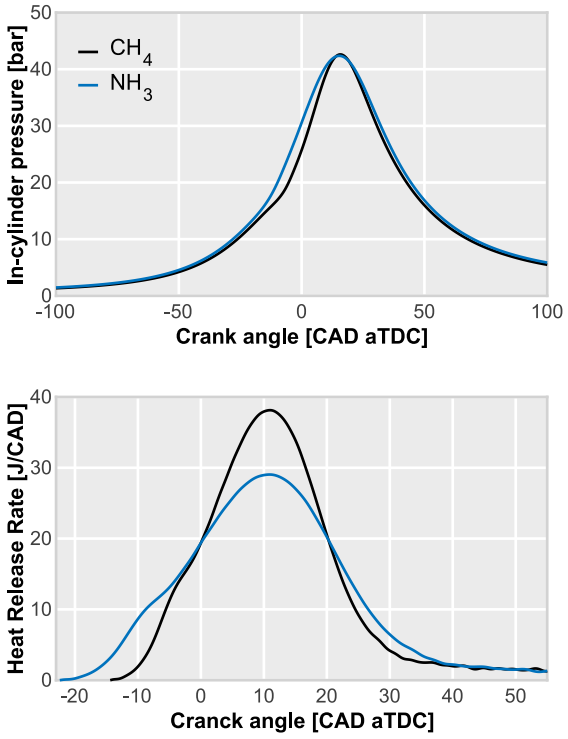

Fig. 8. Combustion process comparison. HRR profiles of methane and ammonia for the operating point number 12.

at 50% of the fuel burnt (CA50) while increasing the combustion duration. For this particular operating point (12), the CA50 was around 10.2 CAD aTDC while the start of combustion was advanced from −14.2 to −22.4 CAD. This requirement has been widely reported in previous research works, as highlighted by Mounaïm-Rousselle et al. [49].

Although the operating constraints are not strictly equivalent to those used in the work of Lhuillier et al. [15], a qualitative comparison can be made to further validate the model. Their results evince a slight indicated efficiency increase when switching from methane to ammonia fuels. This variation is in line with the results obtained. This difference is even higher at increased intake pressures. Therefore, results are completely aligned with the Lhuillier's findings. Nevertheless, the quantitative differences can be explained by the distinct engine platforms, test bench design and operating constraints.

Lastly, Fig. 9 presents the results of the indicated specific fuel consumption (ISFC), providing an insight into the expected consumption values throughout the engine map when operating with ammonia. These values are comparable to those of current diesel or gasoline engines.

4.1.1. *Knocking combustion and potential efficiency gains*

It is interesting to note from Fig. 5(b) how the anti-knocking control used at high loads and low engine speeds in the experiments (e.g. operating point number 12) is compromising the efficiency levels. This control strategy delays the spark timing moving the combustion phasing towards the expansion stroke, avoiding thus abnormal knocking combustion while negatively affecting efficiency levels. Due to the imposition of the same settings of methane-fuelled experiments on the ammonia simulations, the efficiency levels in this region can be increased due to the higher knocking resistance of ammonia.

In order to shed some light on this a complete thermodynamic analysis of the engine cycle is performed. The operating point number

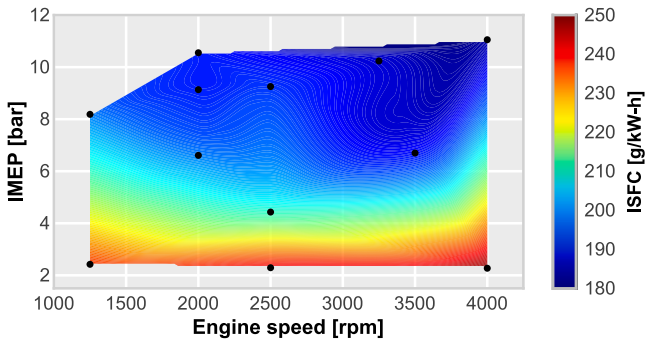

Fig. 9. ISFC values obtained through the operation map using ammonia as fuel.

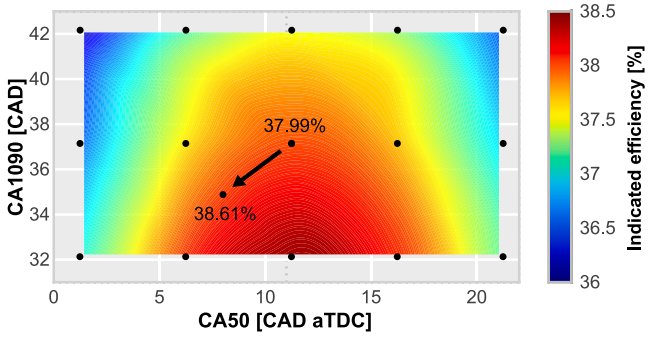

Fig. 10. Indicated efficiency maps obtained from the sensitivity analysis of combustion parameters CA50 and CA1090.

12 is specifically selected for this purpose. During the compression and expansion phases, the cycle efficiency is mostly governed by the polytropic coefficient of the air-fuel mixture [50]. This parameter describes the heat losses during the compression and expansion processes in the thermodynamic cycle of internal combustion engines. It was found that the variation of this coefficient between both mixtures during compression and expansion phases was negligible. For instance, immediately after the intake valves closing (IVC), the polytropic coefficient varies from 1.38 to 1.36 when replacing methane by ammonia. These values where estimated from CFD model data, which utilizes thermodynamic properties of the relevant species included in the chemical mechanisms of Smith et al. [51] and Otomo et al. [46], respectively. Therefore, a substantial increase in efficiency may only be achieved during the combustion phase. Hence, identifying the influence of the duration (CA1090) and phasing (CA50) of combustion on thermal efficiency can help to identify possible room of improvement.

To this end, a sensitivity analysis of both parameters was performed by modifying the combustion phasing and duration through the HRR profile handling. The study consist of a full factorial design based on sweeping both parameters from the reference point (the original ammonia combustion profile of point 12). The CA50 parameter was swept from 1.2 to 21.2 CAD aTDC (crank angle degree after top dead center) while the CA1090 ranges from 32 to 42 CAD.

Results of this study are summarized in Fig. 10, where the indicated efficiency levels are depicted as a function of both parameters. As it can be seen, efficiency levels have a higher dependence on combustion phasing than on combustion duration (CA1090), indicating the critical role of the spark timing. The maximum values are reached at CA50 of 11 CAD aTDC and CA1090 around 32 CAD.

Despite the utility of this study, some relevant phenomena is not considered due to limitations on the combustion modelling approach. Events such as abnormal combustion due to the mixture auto-ignition (knocking) or combustion instability due to misfiring cannot be taken into account. Thus, the expected efficiency gains make no sense without considering these phenomena.

Focusing on this particular case, combustion instabilities do not seem to be a relevant problem since combustion is reasonably phased at top dead center where thermodynamic conditions favour flame propagation. At these conditions, knocking phenomenon is the main constraint, increasing the possibility of engine damage. In order to verify that the efficiency values estimated in the sensitivity study make sense, a predictive combustion modelling approach based on computational fluid dynamics model was used. This model uses the real geometric features of the engine in combination of the boundary conditions representative of the operating point 12 to estimate the evolution of combustion, considering both flame propagation and auto-ignition.

Using this model, the start of combustion is swept through the spark activation to find the optimum combustion phasing without relevant knocking issues. The result of this study is included in Fig. 10, in which the realistic efficiency gain estimated by CFD is depicted. As it can be seen the indicated efficiency increases from 37.9% (reference settings of point 12) to 38.6% (new settings estimated by CFD). In these conditions, combustion phasing (CA50) changes from of 11.2 to 9.3 CAD aTDC, whereas the combustion duration (CA1090) is reduced from 37.1 to 34.9 CAD. This marginal gain in terms of efficiency can be explained by the fact that methane has also a high octane number, hindering the knock appearance. On the contrary, this gain should be more significant if compared with other conventional fuels (e.g. gasoline).

Fig. 11 allows to visualize the non-existence of auto-ignition downstream the flame when using the new settings. Here, the evolution of the flame front can be observed through a sequence of snapshots. The reaction regions are computed by clipping the temperature field between 1800 and 2400 K and then, coloured by the turbulent flame speed. This representation is applied to CA10, CA25, CA50 and CA75 (combustion after 10%, 25%, 50% and 75% of fuel burnt, respectively).

As it can be observed, the flame propagation was progressive and no hot spots arise downstream the flame, even at later combustion phases where the flame velocity is considerably low. Thus, the knocking phenomena is no a real constraint in this particular engine and critical operating conditions (low speed and high engine load). These results are completely aligned with the literature since the work of Koike et al. [52] demonstrated that no knocking occurred at 800 rpm conditions with a compression ratio of 14:1 and boosting up to 2.2 bar. This conclusion increases the possibilities of increasing efficiency ammonia-fuelled engines using strategies that are traditionally limited by knocking phenomenon. For example, increasing the compression ratio, rising the in-cylinder temperature or the turbulence intensity to stabilize combustion. Some of these strategies will be evaluated in the following sections.

4.1.2. Effects of increasing the compression ratio

In view of the potential benefits of ammonia knocking resistance, increasing compression ratio is one of the strategies worth to be evaluated in the search of higher efficiency. Again, the operating point number 12 is chosen because it is the most restrictive for this purpose. Firstly, the effect of compression ratio is assessed by the numerical methodology used so far (namely simple model). In this way, the observed changes only consider the laminar flame speed variations, without taking into account relevant phenomena such as the self-ignition of the mixture, flame morphology or turbulence. Thus, the virtual engine model is coupled with the predictive combustion modelling approach implemented in the CFD model to consider such relevant phenomena involved in the combustion process. In both scenarios, the combustion phasing was maintained at the optimized value obtained in the previous section when sweeping the compression ratio (CR) (refer to Fig. 10). This approach enables a fair comparison of the potential gains in compression ratio, as the impact of combustion phasing is completely decoupled. However, it is crucial to verify the presence of knock subsequently to

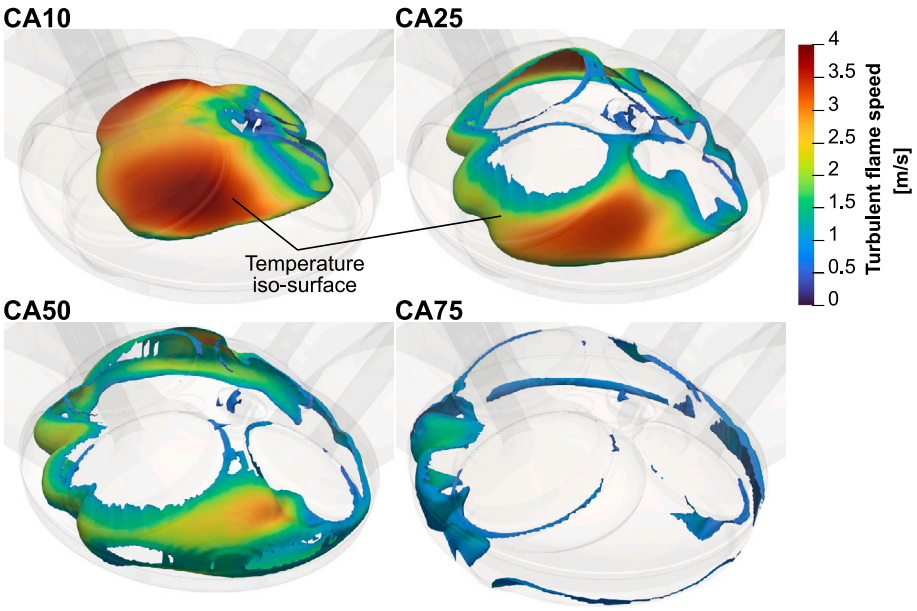

Fig. 11. Combustion process visualization for the operating point 12 with the optimized combustion phasing. The reaction regions are visualized through an iso-surface of temperature clipped by 1800 and 2000 K. (For interpretation of the references to colour in this figure legend, the reader is referred to the web version of this article.)

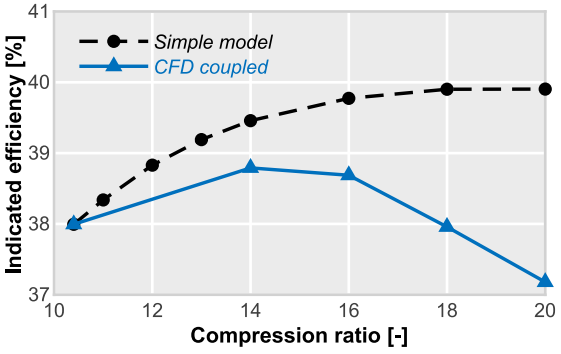

Fig. 12. Impact of increasing compression ratio on indicated efficiency considering two modelling approaches.

ensure that this combustion phasing is realistic from an engine integrity standpoint.

In both cases, the compression ratio is increased from the reference value (10.7:1) up to extreme values (20:1). Fig. 12 summarizes the results of this study, including both modelling approaches. The first modelling approach shows a parabolic growth of the indicated efficiency with a maximum increase of 5%. However, these prospective do not consider all relevant mechanisms affecting the burning rate.

To properly understand the influence of the compression ratio on combustion, it is necessary to address the fundamental aspects governing this process. Mainly, the burning rate depends on thermodynamic conditions inside the chamber, the surface area of the flame front at any given instant and the combustion speed as [50]:

$$\dot{m}_b = \rho_{ub} \cdot A \cdot u_C \tag{4}$$

where ρ_{ub} is the unburned mixture density, A is the surface area of the flame front and u_C is the combustion velocity. Strictly speaking, this first approach only takes into account the density variations and the combustion velocity at least in part since the turbulent velocity is assumed to be constant and everything scales with the laminar flame speed. Therefore, aspects related to the flame front perimeter and the turbulence inside the chamber are neglected. The question lies in how relevant both effects are on the burning rate prediction.

In order of shed some light on this regard, the virtual engine model is coupled with the CFD model, predicting a more realistic scenario where the flame front morphology and turbulence levels are adapted to the modification of the compression ratio. Considering the combustion chamber design of the engine, the piston design was modified by adapting the original piston geometry to the cylinder head as shown in Fig. 13. Considering the substantially high CRs to be evaluated, this is the most direct and reasonable approach. Therefore, the study analyses a realistic scenario that arises if the compression ratio is raised to such high levels in terms of the turbulent flow field, thermo-chemical properties and geometrical features of the flame front.

Recalling trends of Fig. 12, it can be observed the results of the CFD coupled simulations. Indicated efficiency values experience a lower growth than in the previous approach, reaching a maximum gain of 0.8% around 14:1.

To further understand the differences observed between both combustion modelling approaches, the influence of each of the three parameters of Eq. (4) in the burning rate is deeply analysed. To this end, the three parameters and the equivalent burning rate are directly obtained from the CFD model database at the same combustion phasing (e.g. CA50). Results are summarized in Table 7. The burning rate ($\dot{m}_b$) is reduced as the compression ratio is increased. This is representative of the HRR evolution (not included for simplicity) which is decreased with the CR increment, resulting in a slowing down of combustion. Moreover, a significant impact for flame surface (A) and combustion velocity (u_c) is found: around 35% and 12% of reduction respectively when switching from 10.7:1 to 20:1. Fig. 14 shows the same flame front visualization used in Fig. 11 for the different compression ratios at CA50. The reaction regions are visualized by clipping the temperature field between 1800 and 2000 K and coloured by the turbulent combustion velocity. Here, the loss of both flame surface and combustion speed is evident. The reduced chamber volume and the worsened turbulence conditions are conditioning the burning rate and subsequently the thermal efficiency. In contrast, differences in the density of the unburned gases are almost negligible (only 1.2% of variation for the same scenario).

Lastly, Fig. 11 demonstrates that there are no hot spots upstream of the flame, even at the highest compression ratio. This observation implies that the occurrence of knock is not significant under these conditions. Consequently, there is no need to delay the combustion phasing, which would result in higher efficiency penalties.

Fig. 13. Baseline (top) and modified (bottom) piston geometries for the compression ratio study.

Table 7
Parametric analysis of combustion fundamentals when modifying the compression ratio.

CR	$\dot{m}_b$ [g/s]	ρ_{ub} [kg/m^3]	A [cm^2]	u_C [m/s]
10.7:1	6.46	5.97	5.94	1.82
14:1	5.73	5.92	5.56	1.74
16:1	4.53	6.37	4.28	1.66
18:1	4.16	6.14	4.23	1.60
20:1	3.72	6.04	3.86	1.60

All these remarks highlight the need of a dedicated optimization of the combustion system design. On one side, the possibility to achieve higher compression ratios without penalizing combustion due to flame restrictions would lead to a geometrical concept similar to compression ignition engines. In these engines, the piston design and the bowl shape promote a larger flame surface over a longer time span thereby avoiding excessive wall heat transfer loss. In addition, optimizing the internal aerodynamics of the combustion chamber, as well as the intake port design, may contribute to stabilize combustion at high compression ratios.

4.1.3. Effects of increasing the turbulence level

This section analyses the role of turbulence in the combustion process of ammonia. Numerous studies evaluated the relationship between the tumble motion inside the combustion chamber and the turbulence generation, consistently showing that it contributes to increasing the turbulence intensity in the vicinity of the spark plug, as well as homogenizing the turbulent velocity field [53]. High turbulence intensity and moderate convective flux are beneficial from the point of view of increasing combustion velocity, consequently reducing the combustion duration. However, excessive convective flux could lead to flame quenching and flame front stabilization problems.

The influence of tumble motion on the combustion process is evaluated through the CFD model. For simplicity, the tumble level in the combustion chamber is artificially modified by numerically changing the angular velocity of flow at the intake valves closing (IVC). In this sense, the design of the piston and intake ports is frozen to avoid costly simulation tests to achieve the desired effect on the flow. The operating point number 12 was chosen as the reference for the analysis, keeping the same start of combustion.

Fig. 15 shows the reduction of combustion duration (CA1090) against the tumble ratio level. This later parameter was computed at the Bottom Dead Center (BDC) prior to the compression stroke [54]. In addition, the CA1090 was normalized respect to the original CA1090 obtained from the reference operating point 12. Results show up to 30% shorter combustion duration when the tumble ratio increases above 1. While this improvement in burn rate may not translate into substantial performance gains when the combustion phasing is maintained, as illustrated in Fig. 10, it is important to note that it can potentially result in increased overall engine performance and emissions characteristics, particularly in terms of ammonia slip. Furthermore, increasing turbulence levels can influence factors such as combustion stability, and heat transfer, which in turn can impact engine efficiency.

Considering that the reference engine used was not specifically designed for operating with ammonia, the room of improvement in terms of combustion duration is remarkable. This strategy seems to be essential to overcome the difficulties of ammonia combustion stability due to its low combustion speed. Thus, working on combustion chamber and intake ports design optimization should be crucial for the concept.

4.1.4. Effects of increasing the in-cylinder temperature

This section evaluates the influence of in-cylinder temperature on ammonia combustion by the numerical methodology used so far. The idea is to judge if controlling the intake temperature can help to stabilize and accelerates combustion without a significant thermal efficiency loss and knocking combustion problems.

In this study, the operating point 12 fuelled with ammonia was used. The temperature inside the combustion chamber IVC was increased from the reference value up to relatively high values (130 °C) mimicking the effect of increasing the intake temperature through the heat exchanger (intercooler) control. Fig. 16 displays the linear growth of this parameter in the five cases assumed. The in-cylinder temperature at start of combustion (SoC) is also included for analysing the temperature relationship between both instants.

Inspecting the values of laminar flame velocity, an increment about 4 cm/s is observed when the in-cylinder temperature is increased by 36.5 °C at IVC. This marginal growth is consistent with other experimental investigations dedicated to obtaining the laminar flame speed by the outward propagating spherical flame method [48], supporting thus the proposed methodology.

The impact of this laminar flame velocity increase is evaluated by means of combustion duration and indicated efficiency variations. Fig. 17 includes both parameters calculated from the five considered cases. A reduction of 2.5 CAD in terms of combustion duration is observed after increasing the in-cylinder temperature 36.5 °C. This reduction does not result in a significant efficiency improvement. As it can be seen, efficiency levels are virtually constant with a maximum variation of 0.2%.

However, higher temperatures offer advantages for combustion stability. They enhance reaction kinetics, resulting in faster and more complete combustion. Additionally, elevated temperatures facilitate the ignition process, minimizing ignition delays and reducing partial combustion. This, in turn, leads to lower unburned ammonia emissions.

4.2. Combustion of ammonia-hydrogen blends

As previously emphasized, the stability of NH_3 combustion is a paramount aspect of its utilization as a fuel in internal combustion engines. Additionally, its high corrosivity necessitates the regulation of tailpipe NH_3 emissions, even in cases where it is not used as a fuel, due

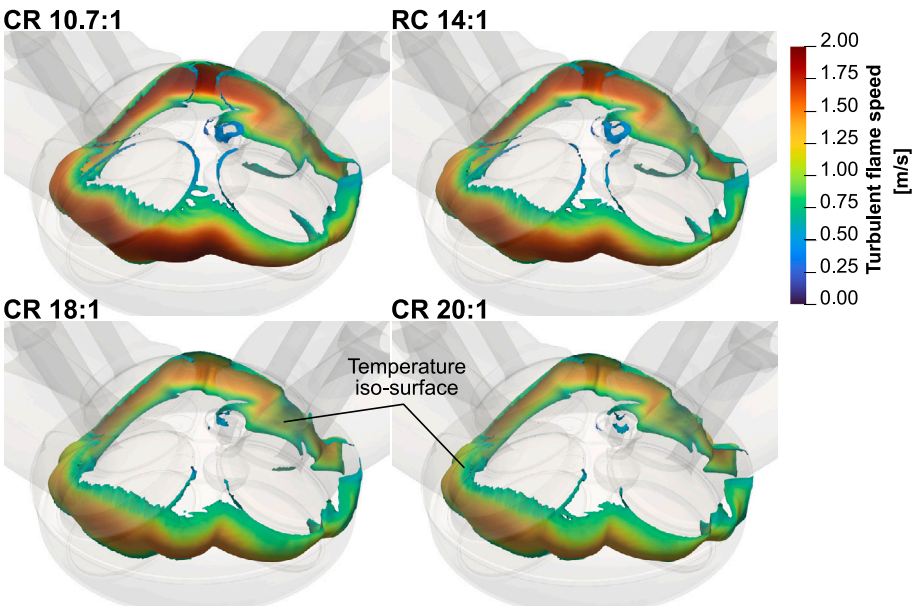

Fig. 14. Combustion process visualization for different compression ratios at CA50. The reaction regions are visualized through an iso-surface of temperature clipped by 1800 and 2000 K.

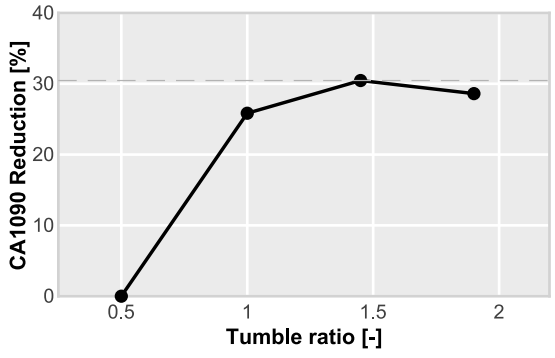

Fig. 15. Effects of tumble ratio on combustion duration (CA1090).

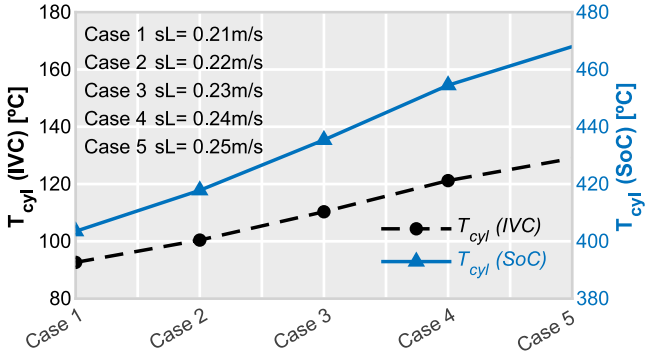

Fig. 16. Impact of in-cylinder temperature on the laminar flame speed of ammonia oxidation. The temperature is computed at IVC and SoC.

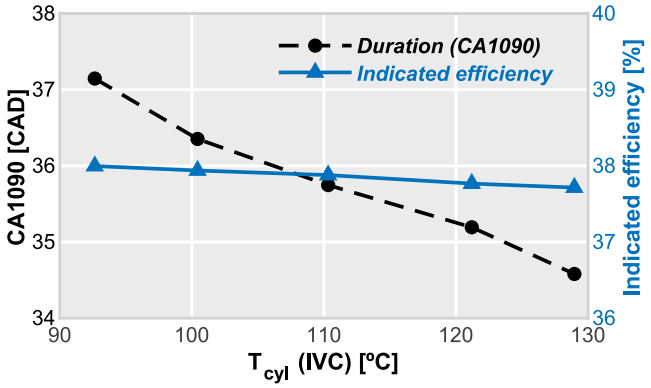

Fig. 17. Effects of increasing the in-cylinder temperature on indicated efficiency and combustion duration.

to its presence in reduction catalysts. Therefore, ammonia combustion stability and evolution are critical considerations when using it as a fuel. Factors such as fuel-air mixing, ignition, flame propagation, and heat release need to be controlled for stable and efficient combustion. Adjusting the fuel reactivity through hydrogen substitution has proven to be a promising approach for controlling ammonia combustion stability and evolution. This strategy is particularly intriguing as the necessary hydrogen can be generated on-board through the dissociation of ammonia [19].

This final section explores the potential use of hydrogen as a combustion enhancer, focusing on engine operating parameters and performance gains. However, it does not delve into the fundamental aspects that influence combustion stability, as analyzing these factors would require costly experiments or simulations conducted in controlled environments that may not fully represent real-world engine operating conditions [24,55].

The effect of hydrogen addition is evaluated at all operating points included in Table 5. Three different percentages of substitution in mass are considered for this study: 2.5%, 5%, and 10%. The total energy available in the fuel blend is maintained by adjusting the amount of ammonia respect to these percentages while maintaining the overall air-to-fuel ratio ($\lambda = 1$). Results are presented in comparison with validated methane combustion cases in Fig. 18, in which the indicated efficiency values are shown for the different hydrogen percentages.

Inspection of this figure reveals that trends mimic the changes observed for the methane fuel, as happened in the case of pure NH_3. Differences among H_2 percentages remained constant in all operating

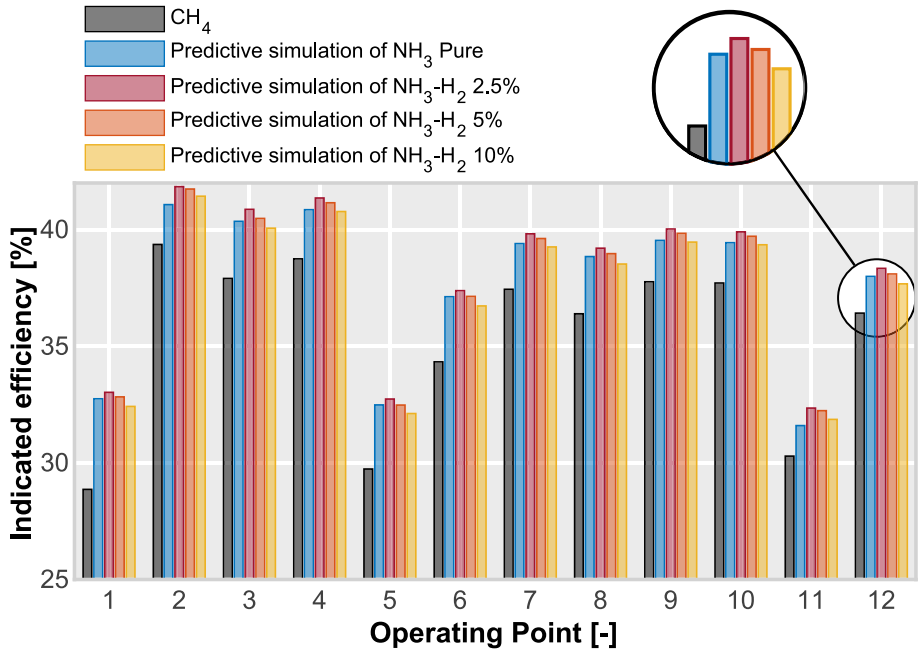

Fig. 18. Indicated efficiency trends for CH_4, NH_3, NH_3 + H_2 2.5%, NH_3 + H_2 5% and NH_3 + H_2 10% fuel blends.

points compared to pure ammonia simulations. In addition, there is a slight increment of efficiency for hydrogen blends below 5%, reaching the maximum efficiency levels for 2.5% of hydrogen substitution. The opposite trend appears as the amount of hydrogen increased significantly (up to 10%), resulting in an overall decrease in the indicated efficiency. This tendency was already observed by Mørch et al. [56]. They observed that the indicated efficiency decreases in blends with higher percentages of hydrogen. This is mainly due to the wall heat loss associated with higher flame temperatures.

One of the primary drawbacks of utilizing hydrogen as a fuel in port injection systems is the significant amount of air displacement in the intake ports caused by its low density. This adversely affects volumetric efficiency, which impacts engine performance due to a higher boost demand. Despite the relatively small mass of hydrogen used in this study, the volume displaced in the intake can still be substantial, even for values below 5% by mass. It is worth noting that employing 3% H_2 in relation to the total fuel mass results in a 20% increase in volume.

Fig. 19(a) illustrates the variation in intake pressure as the percentage of hydrogen in the mixture increases. Surprisingly, the difference between the extreme values is not significant at any of the operating points. To understand this observation, it is necessary to analyze the total mass injected, the corresponding injection volume, and the energy content of the injected mixture. As depicted in Fig. 19(b), the total mass injected decreases rapidly with an increasing proportion of hydrogen in the mixture. Notably, when 10% of ammonia is replaced by hydrogen, the total mass injected decreases by nearly 35%. This reduction is primarily attributed to the substantial difference in LHV between the two fuels (18.6 vs. 120 MJ/kg), while the total injected energy remains constant (Fig. 19(c)). Consequently, the volume displaced in the intake increases by only 10% in the worst-case scenario as depicted in Fig. 19(d). Therefore, the expected variations in injection pressure when operating with NH_3 and H_2 mixtures are relatively low and do not pose a significant issue from the perspective of the boosting system.

In view of these results, enriching with small H_2 percentages (by mass) seems to be an interesting strategy to improve combustion stability and engine efficiency. However, special attention should be paid to the optimization of auxiliary systems (specifically the intake boosting system) as highlighted in the previous section.

5. Conclusions

In this work, a new modelling methodology for spark-ignition engines fuelled by ammonia is proposed based on engine virtualization and detailed CFD simulations. The objective was to further understand the fundamental aspects which govern ammonia combustion in internal combustion engines.

Results are validated against experiments of previous investigations. They also corroborate former research observations extending its application at wider operational ranges along with the identification of keys to achieve a correct operation and/or implementation in spark-ignition engines.

The main conclusions can be summarized as follows:

- Simulations of ammonia-fuelled SI engine showed consistent and comparable results in terms of indicated efficiency against methane combustion over a wide range of operating points.
- It would be necessary to specifically optimize the intake boosting system for ammonia and hydrogen-enriched ammonia operation to obtain comparable results to those of methane operation.
- During the analysis of the compression ratio effect, results showed the influence of flame front surface and turbulence field on the engine efficiency, highlighting the need to optimize the conventional SI combustion system design paradigm for ammonia operation. The optimum compression ratio was around 14:1 for this particular engine operating with ammonia.
- The relevance of the intake port and combustion chamber designs has been evinced. In this way, it is possible to increase the turbulence intensity and, consequently shortening the combustion process while improving efficiency, always taking into account other limitations such as flame quenching due to excessive convective flows. The analysis revealed that increasing the turbulent kinetic energy through the tumble motion resulted in a 30% faster combustion.
- An increase in the in-cylinder temperature in ammonia applications helps to shorten combustion through achieving higher laminar flame speeds. However, this combustion enhancement does not significantly impacts on the engine efficiency. A reduction of approximately 7% in terms of combustion duration (CA1090) was obtained after increasing the in-cylinder temperature by 40% (at the IVC).

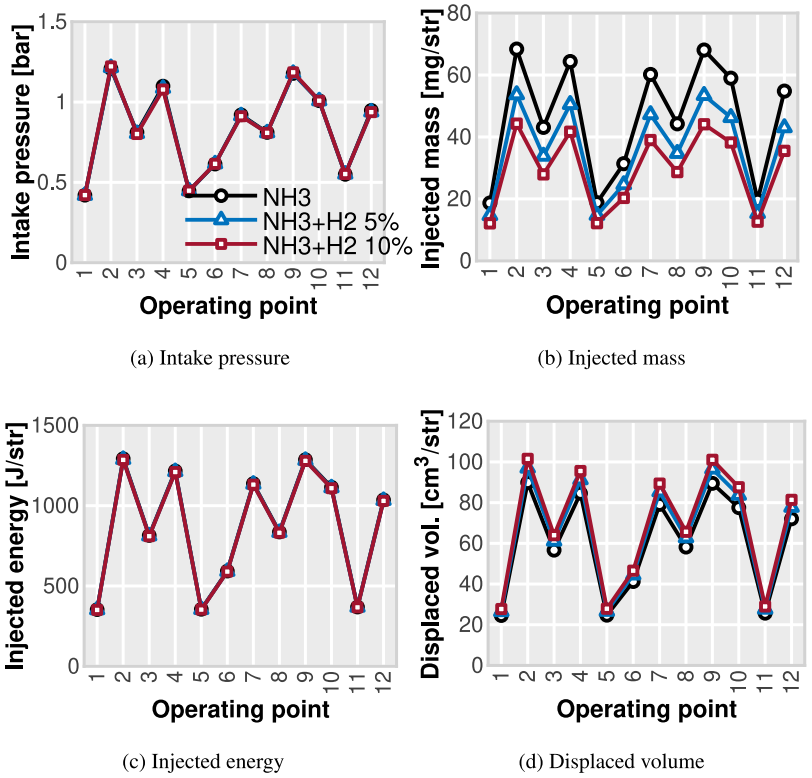

(a) Intake pressure (b) Injected mass

(c) Injected energy (d) Displaced volume

Fig. 19. Boosting and injection flow characteristics of different ammonia/hydrogen fuel blends.

- Marginal gains of efficiency were found when enriching ammonia with hydrogen, offering maximum efficiency levels for 2.5% H_2 blends (by mass).

CRediT authorship contribution statement

R. Novella: Supervision, Funding acquisition, Conceptualization. **J. Pastor:** Writing – review & editing, Methodology, Conceptualization. **J. Gomez-Soriano:** Writing – review & editing, Writing – original draft, Supervision, Project administration. **J. Sánchez-Bayona:** Writing – original draft, Methodology, Data curation.

Declaration of competing interest

The authors declare that they have no known competing financial interests or personal relationships that could have appeared to influence the work reported in this paper.

Data availability

Data will be made available on request.

Acknowledgements

The authors want to express their gratitude to CONVERGENT SCIENCE Inc. and Convergent Science GmbH for their kind support for the 0D, 1D, and CFD calculations with the CONVERGE software.

Funding

Funding for open access charge: CRUE-Universitat Politècnica de València.

Appendix A. Supplementary data

Supplementary material related to this article can be found online at https://doi.org/10.1016/j.fuel.2023.128945.

References

[1] Easterbrook DJ. Greenhouse gases. In: Evidence-based climate science: data opposing co2 emissions as the primary source of global warming: second edition. 2016, p. 163–73. http://dx.doi.org/10.1016/B978-0-12-804588-6.00009-4.

[2] Fuel Cells and Hydrogen Joint Undertaking (FCH). Hydrogen roadmap Europe: A sustainable pathway for the European energy transition. Luxembourg: Publications Office of the European Union; 2019, p. 70.

[3] Change IC, et al. Mitigation of climate change. Contribution of working group III to the fifth assessment report of the intergovernmental panel on climate change, 1454, 2014.

[4] Kreith F, West RE. Fallacies of a hydrogen economy: A critical analysis of hydrogen production and utilization, energy conversion and resources 2004: fuels and combustion technologies, energy. Nucl Eng 2004;203–19.

[5] Berry GD, Aceves SM. The case for hydrogen in a carbon constrained world. J Energy Resour Technol Trans ASME 2005;127(2):89–94. http://dx.doi.org/10.1115/1.1924566.

[6] Ball M, Weeda M. The hydrogen economy - vision or reality? Int J Hydrogen Energy 2015;40(25):7903–19. http://dx.doi.org/10.1016/j.ijhydene.2015.04.032.

[7] Chapman A, Itaoka K, Hirose K, Davidson FT, Nagasawa K, Lloyd AC, Webber ME, Kurban Z, Managi S, Tamaki T, et al. A review of four case studies assessing the potential for hydrogen penetration of the future energy system. Int J Hydrogen Energy 2019;44(13):6371–82.

[8] Law CK, Kwon OC. Effects of hydrocarbon substitution on atmospheric hydrogen-air flame propagation. Int J Hydrogen Energy 2004;29(8):867–79. http://dx.doi.org/10.1016/j.ijhydene.2003.09.012.

[9] Bouaboula H, Ouikhalfan M, Saadoune I, Chaouki J, Zaabout A, Belmabkhout Y. Addressing sustainable energy intermittence for green ammonia production. Energy Rep 2023;9:4507–17.

[10] National Institute of Standard and Technology. One extra reference NIST chemistry WebBook, SRD 69, thermophysical properties of fluid systems.. 2020, URL http://webbook.nist.gov/chemistry/fluid/.

[11] Dimitriou P, Javaid R. A review of ammonia as a compression ignition engine fuel. Int J Hydrogen Energy 2020;45(11):7098–118. http://dx.doi.org/10.1016/j.ijhydene.2019.12.209.

[12] Kobayashi H, Hayakawa A, Somarathne KDA, Okafor EC. Science and technology of ammonia combustion. Proc Combust Inst 2019;37(1):109–33. http://dx.doi.org/10.1016/j.proci.2018.09.029.

[13] Valera-Medina A, Xiao H, Owen-Jones M, David WI, Bowen PJ. Ammonia for power. Prog Energy Combust Sci 2018;69:63–102. http://dx.doi.org/10.1016/j.pecs.2018.07.001.

[14] Frankl S, Gleis S, Karmann S, Prager M, Wachtmeister G. Investigation of ammonia and hydrogen as CO2-free fuels for heavy duty engines using a high pressure dual fuel combustion process. Int J Engine Res 2021;22(10):3196–208.

[15] Lhuillier C, Brequigny P, Contino F, Rousselle C. Combustion characteristics of ammonia in a modern spark-ignition engine. SAE Tech Pap 2019;(October). http://dx.doi.org/10.4271/2019-24-0237.

[16] Kurien C, Mittal M. Utilization of green ammonia as a hydrogen energy carrier for decarbonization in spark ignition engines. Int J Hydrogen Energy 2023. http://dx.doi.org/10.1016/j.ijhydene.2023.04.073, URL https://www.sciencedirect.com/science/article/pii/S0360319923018086.

[17] American Society of Heating, Refrigerating and Air-Conditioning Engineers. ASHRAE handbook of refrigeration. 2005.

[18] Christensen CH, Sørensen Z, Johannessen T, Quaade UJ, Honkala K, Elmøe TD, Nørskov JK. Metal ammine complexes for hydrogen storage. J Mater Chem 2005;15:4106–8. http://dx.doi.org/10.1039/b511589b.

[19] Clark D, Malerd-Fjeld H, Budd M, Yuste-Tirados I, Beeaff D, Aamodt S, Nguyen K, Ansaloni L, Peters T, Vestre PK, Pappas DK, a I Valls M, Remiro-Buenamañana S, Norby T, Bjrheim TS, Serra JM, Kjlseth C. Single-step hydrogen production from NH 3, CH 4, and biogas in stacked proton ceramic reactors. Science 2022;376:390–3.

[20] Devkota S, Shin B-J, Mun J-H, Kang T-H, Yoon HC, Mazari SA, Moon J-H. Process design and optimization of onsite hydrogen production from ammonia: Reactor design, energy saving and NOX control. Fuel 2023;342:127879.

[21] Bozza F, De Bellis V, Malfi E, Teodosio L, Tufano D. Optimal calibration strategy of a hybrid electric vehicle equipped with an ultra-lean pre-chamber SI engine for the minimization of CO2 and pollutant emissions. Energies 2020;13(15):4008.

[22] Meng X, Zhao C, Cui Z, Zhang X, Zhang M, Tian J, Long W, Bi M. Understanding of combustion characteristics and NO generation process with pure ammonia in the pre-chamber jet-induced ignition system. Fuel 2023;331:125743.

[23] Liu Z, Zhou L, Zhong L, Liu P, Wei H. Experimental investigation on the combustion characteristics of NH3/H2/air by the spark ignition and turbulent jet ignition. Combust Sci Technol 2022;1–22.

[24] Tamadonfar P, Arani SK, Kaario O, Vuorinen V. A study of flame dynamics and structure in premixed turbulent planar NH3/H2/Air flames. In: THIESEL conference on thermo-and fluid dynamics of clean propulsion powerplants. 2022.

[25] Yang W, Dinesh KR, Luo K, Thevenin D. Direct numerical simulation of turbulent premixed ammonia and ammonia-hydrogen combustion under engine-relevant conditions. Int J Hydrogen Energy 2022;47(20):11083–100.

[26] Abdelwahid S, Malik MR, Hammoud HAAK, Hernández-Pérez FE, Ghanem B, Im HG. Large eddy simulations of ammonia-hydrogen jet flames at elevated pressure using principal component analysis and deep neural networks. Combust Flame 2023;253:112781.

[27] Wang D, Ji C, Wang S, Yang J, Wang Z. Numerical study of the premixed ammonia-hydrogen combustion under engine-relevant conditions. Int J Hydrogen Energy 2021;46(2):2667–83. http://dx.doi.org/10.1016/j.ijhydene.2020.10.045.

[28] Xin G, Ji C, Wang S, Hong C, Meng H, Yang J. Experimental study on the effect of hydrogen substitution rate on combustion and emission characteristics of ammonia internal combustion engine under different excess air ratio. Fuel 2023;343:127992.

[29] Xin G, Ji C, Wang S, Hong C, Meng H, Yang J, Su F. Experimental study of the effect of variable valve timing on hydrogen-enriched ammonia engine. Fuel 2023;344:128131.

[30] Mounaïm-Rousselle C, Mercier A, Brequigny P, Dumand C, Bouriot J, Houillé S. Performance of ammonia fuel in a spark assisted compression ignition engine. Int J Engine Res 2022;23(5):781–92.

[31] Lhuillier C, Brequigny P, Contino F, Mounaïm-Rousselle C. Experimental study on ammonia/hydrogen/air combustion in spark ignition engine conditions. Fuel 2020;269(February). http://dx.doi.org/10.1016/j.fuel.2020.117448.

[32] Benajes J, Novella R, Gomez-Soriano J, Martinez-Hernandiz PJ, Libert C, Dabiri M. Evaluation of the passive pre-chamber ignition concept for future high compression ratio turbocharged spark-ignition engines. Appl Energy 2019;248(March):576–88. http://dx.doi.org/10.1016/j.apenergy.2019.04.131.

[33] Payri F, Olmeda P, Martin J, Carreño R. A new tool to perform global energy balances in DI diesel engines. SAE Int J Engines 2014;7(1):43–59. http://dx.doi.org/10.4271/2014-01-0665.

[34] Olmeda P, Martín J, Arnau FJ, Artham S. Analysis of the energy balance during world harmonized light vehicles Test Cycle in warmed and cold conditions using a Virtual Engine. Int J Engine Res 2020;21(6):1037–54. http://dx.doi.org/10.1177/1468087419878593.

[35] Molina S, Novella R, Gomez-Soriano J, Olcina-Girona M. New combustion modelling approach for methane-hydrogen fueled engines using machine learning and engine virtualization. Energies 2021;14(20). http://dx.doi.org/10.3390/en14206732.

[36] Molina S, Novella R, Gomez-Soriano J, Olcina-Girona M. Experimental evaluation of methane-hydrogen mixtures for enabling stable lean combustion in spark-ignition engines for automotive applications. SAE technical paper 2022-01-0471, 2022, http://dx.doi.org/10.4271/2022-01-0471.

[37] CONVERGE 2.4 theory manual. CONVERGENT SCIENCE Inc.; 2018.

[38] Scarcelli R, Wallner T, Sevik J, Richards K, Pomraning E, Senecal PK. Cycle-to-cycle variations in multi-cycle engine RANS simulations. In: SAE 2016 world congress and exhibition. SAE International; 2016, http://dx.doi.org/10.4271/2016-01-0593.

[39] Broatch A, Olmeda P, Margot X, Gomez-Soriano J. Numerical simulations for evaluating the impact of advanced insulation coatings on H2 additivated gasoline lean combustion in a turbocharged spark-ignited engine. Appl Therm Eng 2019;148:674–83. http://dx.doi.org/10.1016/j.applthermaleng.2018.11.106.

[40] Issa RI. Solution of the implicitly discretised fluid flow equations by operator-splitting. J Comput Phys 1986;62(1):40–65.

[41] Yakhot V, Orszag SA. Renormalization group analysis of turbulence. I. Basic theory. J Sci Comput 1986;1(1):3–51.

[42] Peters N. Turbulent combustion. IOP Publishing; 2001.

[43] Amsden A, O'Rourke P, Butler T. A computer program for chemically reactive flows with sprays, los alamos laboratory. Technical report, 1989.

[44] Redlich O, Kwong JN. On the thermodynamics of solutions. V. An equation of state. Fugacities of gaseous solutions. Chem Rev 1949;44(1):233–44.

[45] Ewald J, Peters N. A level set based flamelet model for the prediction of combustion in spark ignition engines. In: 15th international multidimensional engine modeling user group. Detroit, MI; 2005.

[46] Otomo J, Koshi M, Mitsumori T, Iwasaki H, Yamada K. Chemical kinetic modeling of ammonia oxidation with improved reaction mechanism for ammonia/air and ammonia/hydrogen/air combustion. Int J Hydrogen Energy 2018;43(5):3004–14.

[47] Aziz M, Wijayanta AT, Nandiyanto ABD. Ammonia as effective hydrogen storage: A review on production, storage and utilization. Energies 2020;13(12). http://dx.doi.org/10.3390/en13123062.

[48] Lhuillier C, Brequigny P, Lamoureux N, Contino F, Mounaïm-Rousselle C. Experimental investigation on laminar burning velocities of ammonia/hydrogen/air mixtures at elevated temperatures. Fuel 2020;263:116653. http://dx.doi.org/10.1016/j.fuel.2019.116653.

[49] Mounaïm-Rousselle C, Brequigny P. Ammonia as fuel for low-carbon spark-ignition engines of tomorrow's passenger cars. Front Mech Eng 2020;6. http://dx.doi.org/10.3389/fmech.2020.00070.

[50] Heywood JB. Internal Combustion Engine Fundamentals. McGraw-Hill; 1988.

[51] Smith GP, Golden DM, Frenklach M, Moriarty NW, Eiteneer B, Goldenberg M, Bowman CT, Hanson RK, Song S, Gardiner WC, Lissianski VV, Qin Z. GRI-mech 3.0. 1999, URL http://www.me.berkeley.edu/gri_mech/.

[52] Koike M, Miyagawa H, Suzuoki T, Ogasawara K. Ammonia as a hydrogen energy carrier and its application to internal combustion engines. 2012, p. 61–70. http://dx.doi.org/10.1533/9780857094575.2.61.

[53] Lienemann H, Shrimpton JS. In-cylinder tumble flow characteristics and implications for fuel/air mixing in direct injection gasoline engines. 2003.

[54] Torregrosa AJ, Broatch A, Margot X, Gomez-Soriano J. Understanding the unsteady pressure field inside combustion chambers of compression-ignited engines using a computational fluid dynamics approach. Int J Engine Res 2020;21(8):1273–85.

[55] Yang X, Solomon A, Kuo T-W. Ignition and combustion simulations of spray-guided SIDI engine using Arrhenius combustion with spark-energy deposition model. SAE technical paper, 2012.

[56] Mrch C, Bjerre A, Gttrup M, Sorenson S, Schramm J. Ammonia/hydrogen mixtures in an SI-engine: Engine performance and analysis of a proposed fuel system. Fuel 2011;90(2):854–64. http://dx.doi.org/10.1016/j.fuel.2010.09.042.